Filling of a water-free void explains the allosteric regulation of the β_1-adrenergic receptor by cholesterol

Layara Akemi Abiko,[1,†*] Raphael Dias Teixeira,[1,†] Sylvain Engilberge,[2,3] Anne Grahl,[1] Tobias Mühlethaler,[1] Timothy Sharpe,[1] and Stephan Grzesiek[1*]

[1]Biozentrum, University of Basel, CH-4056 Basel, Switzerland

[2]Paul Scherrer Institut, Forschungsstrasse 111, Villigen PSI, 5232, Switzerland

[3]Present address: European Synchrotron Radiation Facility, F-38043 Grenoble, France

[†]These authors contributed equally

This version of the article has been accepted for publication, after peer review but is not the Version of Record and does not reflect post-acceptance improvements, or any corrections. The Version of Record is available online at: http://dx.doi.org/10.1038/s41557-022-01009-9. Use of this Accepted Version is subject to the publisher's Accepted Manuscript terms of use https://www.springernature.com/gp/open-research/policies/accepted-manuscript-terms.

*Address correspondence to:
Layara Abiko
Biozentrum, University of Basel
CH-4056 Basel, Switzerland
Phone: ++41 61 267 2100
FAX: ++41 61 267 2109
Email: layaraakemi.abiko@unibas.ch

Stephan Grzesiek
Biozentrum, University of Basel
CH-4056 Basel, Switzerland
Phone: ++41 61 267 2100
FAX: ++41 61 267 2109
Email: Stephan.Grzesiek@unibas.ch

Keywords: allosteric regulation; G protein-coupled receptor; β_1-adrenergic receptor; cholesterol; xenon; structural biology.

ABSTRACT

Recent high-pressure NMR results indicate that the preactive conformation of the β_1-adrenergic receptor (β_1AR) harbors completely empty cavities of about ~100 Å^3 volume, which disappear in the active conformation of the receptor. Here we have localized these cavities by X-ray crystallography of xenon-derivatized β_1AR crystals. One of the cavities is in direct contact with the cholesterol binding pocket. Solution NMR shows that addition of the cholesterol analog cholesteryl hemisuccinate impedes the formation of the active conformation of detergent-solubilized β_1AR by blocking conserved G protein-coupled receptor microswitches, concomitant with an affinity reduction of both isoprenaline and G protein-mimicking nanobody Nb80 for β_1AR detected by isothermal titration calorimetry. This wedge-like action explains the function of cholesterol as a negative allosteric modulator of β_1AR. The detailed understanding of GPCR regulation by cholesterol via filling of a dry void and the easy scouting for such voids by xenon may provide new routes for the development of allosteric drugs.

INTRODUCTION

The interiors of experimentally determined protein structures often contain cavities, which are not filled by protein atoms. Such cavities may or may not be occupied by water[1–3], which is often hard to decide due to the difficulties in detecting the highly mobile[3] water molecules in protein interiors. Hydrophilic cavities are highly likely to be hydrated with water, which makes hydrogen bonds to the protein[1,2]. Hydrophobic cavities are much less likely to be hydrated, but the complete absence of water is difficult to prove. Several cases of partially or completely empty hydrophobic cavities have been unambiguously identified using X-ray crystallography or NMR spectroscopy[4–7]. These observations are so far limited to a few model systems, and it is unclear to what extent such dry voids are connected to protein function and structural stability.

Recent high-pressure NMR analysis has shown that such a functional role exists in G protein-coupled receptors (GPCRs)[8]. GPCRs are transmembrane proteins that regulate many vital functions of the human body, and as such are highly attractive drug targets. They recognize a variety of extracellular stimuli and subsequently trigger intracellular downstream signaling cascades[9]. GPCR function is achieved by a high intrinsic flexibility, which allows the interchange between several conformations encoding inactive and active states[10–18]. Notably, the static, crystallographic structures of binary GPCR complexes with agonists and antagonists in the absence of a G protein or a G protein mimetic are very similar and do not reflect their functional difference[17]. In contrast, NMR has shown that the binary agonist·receptor complexes, but not the antagonist·receptor complexes, are in a dynamical equilibrium between a preactive and an active conformation[10]. The active conformation largely corresponds to the conformation in ternary complexes with G protein or G protein-mimicking nanobodies (Nbs) where transmembrane helices (TM) 5 and 6 have moved outward to accommodate the G protein/Nb[19] and the water-mediated H-bond bridge between $Y^{5.58}$ and $Y^{7.53}$ (YY-lock, superscripts indicate Ballesteros−Weinstein numbering[20]) is closed[10,21]. In contrast, the preactive conformation of the agonist complex largely resembles the inactive conformation of antagonist complexes with an open YY-lock[10]. G protein recognition of agonist-

receptor complexes apparently occurs by conformational selection of the active conformation.

The conformational equilibria of GPCRs are sensitive to many factors, for example point mutations, pressure and the lipid environment. Point mutations, introduced to stabilize the β_1-adrenergic receptor (β_1AR) for structural studies, increase the melting temperature in detergent micelles by up to ~30 ˚C, but shift the equilibria towards an inactive receptor[11,22–25]. In particular, mutations of the highly conserved[26,27] Y227$^{5.58}$ and Y343$^{7.53}$ residues, increase the melting temperature by 11 ˚C, but suppress the formation of the active conformation in binary agonist complexes thereby abrogating G-protein binding[10,11].

We have recently shown that pressure modulates these conformational equilibria in the less thermostabilized β_1AR mutant YY-β_1AR[8], which retains the two tyrosines Y227$^{5.58}$ and Y343$^{7.53}$ and is capable of G protein binding. When subjected to pressure (midpoint ~600 bar), YY-β_1AR is shifted from a mixture of preactive and active conformations to a fully populated active conformation even in the absence of a G protein or G protein-mimicking nanobody. This pressure dependence shows that the active conformation has an about 100 Å^3 smaller volume than the preactive conformation, which must be due to the collapse of empty (not water-filled) cavities within the receptor-detergent micelle.

An important, extrinsic factor modulating GPCR conformational equilibria are lipids, with cholesterol (CLR) being the most explored[28–32]. CLR is highly abundant in human cells and is essential for maintaining cell excitability and homeostasis[32–40]. CLR increases GPCR thermal stability[41–47] and often acts as an allosteric modulator of GPCR activity[48–53]. The direction of modulation can vary, as CLR e.g. stabilizes the inactive state of CCK1R[49] and the active state of BLT2R[52]. The molecular mechanisms of such effects are not well understood. They may result from direct interactions with receptors, as observed in multiple GPCR crystal structures[54–61], or more indirectly by a modulation of membrane physical properties such as fluidity and stiffness which could influence the conformational equilibria and spatial organization of the receptor[36,62–65].

As CLR is highly insoluble, commonly its more soluble analog, cholesteryl hemisuccinate (CHS) is used in functional and structural studies[46,52]. CHS

induces similar thermo-stabilizing effects as CLR[53] and molecular dynamics simulations show that protonated CHS mimics well many of the membrane modulating properties of CLR[66]. CLR and CHS are the most prevalent lipids resolved in GPCR structures, but often resolution is not high enough to distinguish between the two[40,61]. Although the well-defined localization of CLR/CHS in these structures suggests specific binding, no conserved binding sites have been identified[61], even for closely related GPCRs such as the β_1- and β_2-ARs[54,67,68]. Instead, CLR or CHS appear at multiple sites, usually in shallow grooves between the transmembrane helices or at the receptor surface[32,61].

Hydrophobic voids tend to incorporate noble gases[5]. Here we have detected hydrophobic voids in β_1AR using crystallography of xenon-derivatized receptor crystals. One of the identified voids is in direct contact with the CHS binding site. An NMR analysis of the effect of CHS binding to an agonist-β_1AR complex shows that CHS restricts the receptor dynamics and hinders the formation of the active state. Furthermore, CHS reduces the affinity of the agonist for the apo receptor and of the G protein mimicking Nb80 for the agonist-bound receptor. These findings can be rationalized by a careful comparison of β_1AR structures, which reveals that CHS bound to the inactive receptor obstructs the path of subtle, but essential movements required to activate the canonical microswitch GPCR network. Thus, CHS apparently acts like a wedge blocking a void necessary for β_1AR activation. The observed phenomenon of functional dry voids together with the possibility to easily detect such voids by xenon may introduce a valuable new principle to search for relevant drug target sites in proteins.

RESULTS

Xenon reveals empty cavities in agonist-bound β_1AR

To localize the hydrophobic voids within β_1AR, we have obtained crystals of a thermostabilized mutant (TS-β_1AR)[11] bound to the agonist isoprenaline and derivatized these with xenon under low (5–10 bar) pressure. Xenon is easily detected and localized using X-ray crystallography due to its anomalous scattering and large number of electrons[5,69]. As dry xenon immediately destroyed the fragile receptor crystals, the xenon derivatization was carried out in a home-built pressurizing device (Figure 1A), where a defined humidity could be set by flowing xenon through a wash bottle before reaching the crystal pressure chamber. An electronic humidity sensor and a glass window in the crystal pressure chamber allowed continuous monitoring of humidity and crystal integrity under a microscope. The best results with no observable crystal damage were achieved by pressurizing the crystals with xenon for 20 min at 5 bar and 100% relative humidity (4 °C) using pure water as the washing liquid.

The structure of the isoprenaline·β_1AR complex determined from the xenon-derivatized crystals (Table S1) is almost identical to the previously solved structure of a similar β_1AR construct in complex with the same agonist (PDB 2y03)[67] (Figure S1A). Both structures have two receptor molecules in identical arrangement in the asymmetric unit with an overall Cα root-mean-square deviation (RMSD) of 0.705 Å (0.607 Å excluding loops). However, the large anisotropy of the Xe-derivatized crystals prevented localization of the isoprenaline and CHS molecules observed in the 2y03 structure. Two xenon binding sites (Xe1, Xe2) were located unambiguously (signal amplitudes >5σ) within the anomalous scattering Fourier map of each of four different crystals (Figures 1B, C and S1B, Table S2). A refinement of the anomalous scattering density yielded single Xe atom occupancies of 0.15 and 0.18 at sites Xe1 and Xe2, respectively. Xe1 is positioned towards the intracellular side between TM3 and TM4, and Xe2 towards the extracellular side between TM2 and TM3. Both xenon binding sites constitute crevices, which are formed almost exclusively by hydrophobic side chains (Figure S2A, B). A control diffraction on a crystal from

the same crystallization batch without xenon derivatization showed no anomalous scattering signal >5σ (Figure S1B).

A computational search for cavities in the 2y03 isoprenaline·β_1AR structure, with water and detergent molecules (including CHS) removed, revealed 15 voids (Figure 1C), two of which are larger and exposed to water at the extracellular and intracellular faces of the receptor. The remaining cavities are smaller and buried in the hydrophobic membrane part of the receptor. Two of these overlap with the Xe1 and Xe2 sites (Figure 1B, C). An analysis of the computed cavities showed no significant differences of hydrophobicity between the two cavities harboring xenon and the other 11 interior cavities not filled by xenon (Table S3). Thus xenon selectively detects a subset of all interior cavities.

The smaller of the computed voids (~20 Å^3) overlapping with the xenon sites largely coincides with the volume of the Xe2 site detected by the xenon anomalous scattering. The larger void (~35 Å^3) constitutes a hydrophobic groove, which is partially but not completely filled by the CHS molecule in the 2y03 structure (Figure 1C). The detected xenon volume at Xe1 resides in the remaining non-filled part of the groove and is in direct contact with the space occupied by the CHS molecule. Despite not being deeply inserted between the helices, CHS is stabilized by an extensive set of hydrophobic interactions involving TM3, TM4, and TM5 (Figure S2C). Notably, the hydrophilic CHS succinic acid tail is not in direct contact with the receptor, but points towards the solvent thereby leaving the Xe1 part of the hydrophobic groove unoccupied. From this arrangement, it is sterically possible that in the native membrane the sterol moiety of CLR fully occupies the Xe1 pocket.

CHS obstructs pressure-induced receptor activation

To investigate the effect of CHS on the receptor void volumes, we acquired pressure-dependent ^{1}H-^{15}N transverse relaxation optimized spectroscopy (TROSY) spectra of the G protein binding-competent ^{15}N-valine-labelled isoprenaline·YY-β_1AR complex[10,11] in the presence (Figure 2A) and absence (Figure 2B) of CHS. Besides small chemical shift changes and variations in intensity (see below), the valine ^{1}H-^{15}N resonances are very similar at 1 bar with and without CHS. However, when the pressure is increased to 2500 bar, the

spectra diverge strongly. Without CHS, the previously observed[8] pressure-induced change to the active conformation is evident from strong shifts of the V122$^{3.33}$, V172$^{4.56}$, V202^{ECL2}, and V314$^{6.59}$ resonances (Figure 2B) around the orthosteric ligand pocket (see also Figure 3B). In contrast, these active-conformation resonances almost disappear with CHS at 2500 bar. In addition, many of the other resonances are broadened and shifted to the center of the NH spectral region, which is indicative of local unfolding and an exchange between many conformations (Figure 2A, C). Only few resonances, such as V89$^{2.52}$, V103$^{2.66}$, and V320^{ECL3} remain intense, which must be due to either fast exchange between local subconformations or the absence of local heterogeneity. Monitoring the receptor stability from the intensity of amide $^{1}H^{N}$ resonances revealed that the addition of CHS leads to a considerably faster sample decay at 2500 bar, whereas CHS stabilizes the sample at 1 bar (Figure S3). The disappearance of resonances is due to the formation of large NMR-invisible aggregates and precipitation. Taken together these observations show that CHS blocks the activating motion at 2500 bar, and directs the receptor to unstable, presumably partially unfolded conformations that lead to precipitation.

CHS acts as an allosteric inhibitor for β_1AR

The blocking of the isoprenaline·YY-β_1AR active state by CHS is already apparent from a careful comparison of ^{1}H-^{15}N TROSY spectra at 1 bar in the presence and absence of CHS (Figure 3A and S4). Moderate chemical shift changes induced by CHS on V160$^{4.44}$, V129$^{3.40}$ and other nearby valines (Figure 3A,B yellow labels) indicate minor effects on the local conformations of β_1AR by CHS and show that in solution CHS binds to a location on the receptor that is similar to the CHS binding site in the crystal. As observed previously[8,10], the resonances of V172$^{4.56}$, V202^{ECL2}, and V314$^{6.59}$ are split without CHS into a major form and a minor form corresponding to the preactive and active conformations in slow (>5 ms) chemical exchange. Their average intensity ratio corresponds to an active population of ~19% (Figure 3C and S4). In the presence of CHS, the resonances of the active conformation are no longer visible, indicating that its population should be smaller than ~13% using the spectral noise as detection

limit. Thus, CHS appears to shift the preactive-active equilibrium towards the preactive conformation for isoprenaline·YY-β_1AR at ambient pressure.

This CHS-induced equilibrium shift is confirmed by the analysis of a further β_1AR mutant, YY-β_1AR-V129I, in which the thermostabilizing mutation I129$^{3.40}$V was reverted to the native isoleucine. In the isoprenaline·YY-β_1AR-V129$^{3.40}$I complex, the preactive-active conformational equilibrium is strongly shifted towards the active conformation, whereas the conformations of receptor complexes with antagonists remain unchanged (Grahl et al. in preparation). The effect of the I129$^{3.40}$V mutation on the preactive-active equilibrium is apparent in the ^{1}H-^{15}N TROSY spectrum of ^{15}N-valine-labeled YY-β_1AR-V129$^{3.40}$I in complex with isoprenaline in the absence of CHS (Figure 3A). This shows strong active-conformation resonances for V122$^{3.33}$, V172$^{4.56}$, V202^{ECL2}, and V314$^{6.59}$ and almost no preactive-conformation resonances. In contrast, in the presence of CHS, the active-conformation resonances show reduced intensities but remain well observable, whereas the intensities of the preactive-conformation resonances are increased to about the same magnitude. A quantitative analysis of the intensities (Figure 3C) indicates a population of the active conformation larger than ~80% without CHS, whereas this population decreases to ~50% in the presence of CHS. Thus, CHS also shifts the preactive-active equilibrium towards the preactive conformation for the YY-β_1AR-V129$^{3.40}$I mutant in complex with isoprenaline.

Increasing the CHS concentration from 1 to 2 mM further decreased the population of the active conformation for isoprenaline·YY-β_1AR-V129$^{3.40}$I to ~40% (Figure S4) showing that the apparent affinity of the CHS binding site must be in the micro- to millimolar range. In contrast, doubling the concentration of isoprenaline from 2 to 4 mM did not significantly change the preactive-active equilibrium (Figure S4). This indicates that the orthosteric binding site is fully occupied by isoprenaline and argues against the possibility that CHS competes with isoprenaline for the orthosteric site as suggested previously[70]. The binding of low-affinity ligands like CHS may cause broadening of resonances due to intermediate time-scale (micro- to millisecond) exchange. However, CHS does not induce large changes in the line shapes and total integrals of the preactive-

and active-conformation resonances of V122$^{3.33}$, V172$^{4.56}$, V202^{ECL2}, and V314$^{6.59}$, and it also does not affect the resonance intensities and line shapes of other residues such as V89$^{2.52}$ and V103$^{2.65}$, which can be used as a reference. Therefore, the reduced intensities of the active conformation must be due to a true population change and not to a bleaching of resonances from intermediate exchange. Overall, the effects of CHS both on the pressure-dependent β_1AR spectra and on the preactive-active equilibrium at ambient pressure show that CHS apparently acts as an allosteric inhibitor of the internal activating motions of the receptor.

CHS reduces the affinity of both isoprenaline and Nb80 for β_1AR

To further understand the implications of the CHS interaction with β_1AR we performed isothermal titration calorimetry experiments (ITC) with orthosteric and allosteric ligands in the absence and presence of CHS (Figure 5). These titrations revealed that CHS reduces the affinity of isoprenaline for apo YY-β_1AR-V129$^{3.40}$I 6.5-fold (K_D = 11 µM vs 1.7 µM), whereas the affinity of Nb80 for the isoprenaline-bound receptor decreases 2.5-fold (K_D = 107 nM vs 42 nM). These results clearly show the negative allosteric effects of CHS on the biochemical behavior of both the orthosteric and the effector binding sites and are in complete agreement with the NMR findings of inhibition of the active conformation.

Structural basis of β_1AR regulation by CHS

To rationalize this allosteric inhibition mechanism by CHS, we compared the available crystallographic structures of the binary isoprenaline·β_1AR complex in the preactive conformation and the ternary complex of isoprenaline·β_1AR with the G protein-mimicking nanobody Nb80 in the active conformation (Figure 4A). Although CHS was added during the preparation of both complexes[67,71], an ordered CHS molecule is only detected in the binary preactive complex. In the β_1AR preactive conformation, CHS makes extensive, hydrophobic contacts to residues in TM3, TM4 and TM5 (Figure 4A and S2C). In the active state, the intracellular part of TM5 swings out of the helical bundle, but the center and extracellular parts move inward and slide by ~2.5 Å towards the intracellular side (Figure 4A). This would lead to a sterical clash of the I214$^{5.45}$ and I218$^{5.49}$ side

chains with the aliphatic end of CHS in the preactive structure. Similarly, the intracellular part of TM4 in the active structure moves towards the CHS position by 1.5 Å and would cause a clash of V160$^{4.44}$ and T164$^{4.48}$ with the hydrophilic tail of CHS. These clashes of CHS with the active β_1AR conformation may explain the absence of an ordered CHS molecule in the active structure. Besides such repulsive forces, the inactive conformation seems further stabilized by attractive interactions from CHS to residues E130$^{3.41}$, I137$^{3.48}$ and P219$^{5.50}$, which may prevent the inward motion of TM3 and the sliding of TM5 required to reach the active conformation.

Taken together, CHS apparently blocks the motions of TM3-5, which activate the canonical GPCR microswitch signaling network (Figure 4A,B). In particular, these comprise the inward motion of residues I129$^{3.40}$ (PIF motif) and R139$^{3.50}$ (DRY motif) in TM3, which push TM6 outwards via F299$^{6.44}$ and L289$^{6.34}$, as well as the downward motion of Y227$^{5.58}$ in TM5, which enables formation of the conserved YY-lock with Y343$^{7.53}$ (NPxxY motif) in TM7 that stabilizes the swung-out position of TM6[10].

The detected Xe sites are conserved allosteric binding pockets

To further understand the CHS/CLR allosteric mechanism in the context of other GPCRs, we compared our findings with other receptors, which bind synthetic allosteric modulators at the same Xe1 site (Figure 4C,D). The compound AS408 is a negative allosteric modulator (NAM) of β_2AR for both G protein activation and arrestin recruitment[72]. The allosteric inhibition of β_2AR by AS408 can be explained by the same mechanism as the CHS inhibition of β_1AR, that is, AS408 appears to hinder the sliding of TM5 towards the intracellular side and to block the TM3 movement. These are necessary for activation. Although the amino acid sequences of β_2AR and β_1AR are very similar, including the region of this allosteric binding site, the substitution of a single amino acid at position 3.48 (valine in β_2AR and leucine in β_1AR) is sufficient to reduce the affinity of AS408 for β_1AR tenfold relative to β_2AR[72]. This substitution may also be the reason why β_2AR does not bind cholesterol at the same site.

A further comparison with the receptor GPR40 (free fatty acid receptor 1) is particularly interesting, since the binding of the allosteric compound AP8 to the

same site as occupied by CHS in β_1AR induces an upregulation of activity. Thus AP8 is a positive allosteric modulator (PAM) enhancing the response of partial agonists[73]. No active structures of GPR40 are available in complexes with a G protein or G protein mimetic. However, TM5 of the preactive GPR40 in complex with the agonist MK-8666 is shifted towards the intracellular side relative to other active GPCR·G protein complexes (β_2AR, A2R)[73]. Binding of the PAM AP8 to the MK-8666·GPR40 complex then shifts TM5 towards the extracellular side (Figure 4C), i.e., towards the conformation of the active β_2AR and A2R GPCR complexes. Thus, the shift of TM5 from the preactive to the active GPR40 conformation is opposite to the usual direction. The alignment of the binary MK-8666·GPR40 and ternary MK-8666·GPR40·AP8 complexes (Figure 4C) reveals that AP8 would clash with the preactive conformation of TM5, thereby explaining its positive modulation of GPR40 activity, in complete agreement with the negative modulation by CHS and AS408 binding to the same site in β_1AR and β_2AR, respectively.

A further structure, that is, P2Y1R in complex with the inhibiting antithrombotic drug BPTU (PDB 4XNV),[74] also has a CHS molecule bound close to the Xe1 site in β_1AR albeit in a different orientation (Figure 4D). The effect of CHS/CLR on P2Y1R has not been characterized in detail, but P2Y1R-mediated calcium release in platelets was reported as insensitive to CLR depletion[75]. Intriguingly, however, the antithrombotic drug BPTU binds to a second allosteric pocket on the external P2Y1R interface with the lipid bilayer (Figure 4D), which coincides with the Xe2 site in β_1AR. Thus, apparently, albeit detected in a different receptor, the Xe2 site also constitutes a drug binding pocket.

DISCUSSION

Here we have determined and rationalized in atomic detail the effect of CHS onto the β_1AR functional equilibria by a combination of crystallography, solution NMR and ITC experiments. As high pressure shifts the preactive-active conformational equilibrium of the isoprenaline·YY-β_1AR complex to the active conformation, the receptor must compress empty cavities during activation. We have localized two such cavities using X-ray diffraction of Xe-derivatized β_1AR crystals. Two xenon atoms fill these hydrophobic cavities with 15–18%

occupancy. The volume occupied by these xenon atoms (Xe van der Waals volume 42 Å^3) is not directly related to the volume of their surrounding hydrophobic pocket. Thus, a recent study detected one xenon atom with an occupancy of 17% in a hydrophobic pocket of 141 Å^3 volume, which is very similar to our results, but also a second xenon atom with an 68% occupancy in a pocket of only 16-Å^3 volume[5]. Therefore, the volume of the hydrophobic pockets in β_1AR is not well defined by the Xe scattering results, but the range of the hydrophobic volume expected for both Xe sites agrees with the ~100 Å^3 volume difference between the active and the preactive conformations detected by high-pressure NMR[8]. However, further empty cavities may however also exist in β_1AR that escaped detection by xenon due to the low resolution of the crystals or low occupancy. The two detected Xe sites overlap with two of the 13 interior voids derived from a computational analysis of the static β_1AR crystal structure. The noble gases xenon and krypton are known to preferentially bind to desolvated, hydrophobic protein cavities through weak van der Waals interactions[5,76]. However, no correlation is observed between the hydrophobicity of residues lining the voids computed from the static crystal structure and the detected Xe binding. This lack of correlation may be caused by the relatively low resolution of the crystal structure (2.85 Å), but is also very likely to be due to the highly dynamic nature of GPCRs, which may lead to interactions that differ from the expectations of a static structure. By contrast, the experimental detection of Xe binding clearly indicates a relevant interaction.

Intriguingly, one of the Xe-detected cavities colocalizes with the CHS binding site. Our NMR results show that CHS binds to a similar region of the detergent-solubilized receptor as in the crystal structures. Moreover, CHS shifts the preactive-active equilibrium to the preactive conformation and abrogates the pressure-induced switch of the isoprenaline·YY-β_1AR complex to the active conformation. This can be rationalized by CHS filling the cavity required for activation. In complete agreement with these structural findings, the affinities of both isoprenaline and Nb80 for β_1AR are considerably reduced in the presence of CHS, since CHS prevents the active conformation, i.e. the increase of contacts

to isoprenaline via the sliding motion of TM5[10] and the accommodation of Nb80 by the outward movement of TM5 and TM6.

Atomic details of the inhibitory effect of CHS can be derived from a careful comparison of the preactive isoprenaline·β_1AR structure with bound CHS and the active isoprenaline·β_1AR·Nb80 structure, which does not contain detectable CHS. In the binary isoprenaline·β_1AR complex, CHS stabilizes the preactive conformation by numerous hydrophobic interactions. However, CHS would clash with β_1AR TM4 and TM5 atoms in the active conformation. By this mechanism, CHS obstructs functional motions required for the activation of the canonical GPCR microswitch network.

As compared to CHS, even stronger inhibitory effects are expected for CLR due to its larger hydrophobicity and the hydrophobic character of the identified combined Xe- and CHS-binding site. This inhibitory function of CLR is corroborated by the enhanced signaling of α- and β-adrenergic receptors in cardiomyocytes depleted of cellular CLR[77]. Being highly abundant in the cell membrane (34% of the total lipid content in mammalian plasma membranes[35,39]), CLR may be a prime regulator of adrenergic receptors, keeping their basal activity low by stabilizing their preactive conformation. It is also very likely that the activity of many further GPCR is modulated by CLR. For example, CLR was recently shown to act as a positive allosteric modulator of the cannabinoid receptor CB2, since depletion of CLR from the plasma membrane decreases its activity, both in the presence of agonists and in the apo state[78]. As CLR levels vary among different cell types and subcellular compartments, this may introduce an additional layer of cell-specific receptor modulation.

In many cases, the binding of CLR/CHS seems rather specific, since these lipids are detected at specific localizations in crystal structures and also our current data show that CHS binds to the same site in solubilized β_1AR as in the crystal. However, the identified CLR/CHS binding sites are rather diverse across different GPCRs. Therefore, there cannot be a universal mechanism of allosteric GPCR regulation by CLR. Nevertheless, our study reveals two general aspects of the CLR action on GPCRs: (i) by filling cavities, CLR reduces the total volume

available for functional motions and (ii) CLR ties together hydrophobic parts of the receptor thereby stabilizing a particular conformation.

Several allosteric modulators of other GPCRs bind to the same site as CHS in β_1AR. Although their binding site is identical, the functional output may vary. For example, such allosteric modulators increase the activity of GPR40 and DRD1[73,79], but down-modulate β_2AR and C5aR1[72,80]. Blocking TM5 sliding appears as the hallmark of their mechanism of action with the position of the blocked TM5 relative to the active conformation defining the direction of modulation.

The present study adds to the mounting evidence that empty cavities may fulfill key functions in proteins such as the high-affinity binding of hydrophobic ligand moieties[5] or directing functional motions[8]. Apparently, CHS fills a void that must be compressed for β_1AR activation. Filling spaces between the transmembrane helices modulates the dynamics and activity of many GPCRs, as demonstrated by the development of a number of positive and negative allosteric modulators[72–74,79–82], which occupy such crevices. In contrast to the orthosteric binding sites, the surfaces of allosteric binding sites are often lined by amino acids that are distinctive between GPCR subtypes. This property gives them a high potential for the development of therapeutic drugs targeting specific GPCR subtypes.

Intriguingly, not only the detected xenon binding site Xe1 in β_1AR colocalizes with the binding site of the allosteric modulator CHS/CLR, but also Xe2 colocalizes with the antithrombotic drug BPTU in P2Y1R. Therefore, the detection of empty cavities by xenon may provide valuable clues in the search for new drug target sites in GPCRs.

ACKNOWLEDGMENTS

Manuscript first published in *Nature Chemistry*, **14**, 1133-1141 (2022) by Springer Nature.

This work was supported by the Swiss National Science Foundation (Grants CRSK-3_195592 to L.A.A., and 31-149927, 31-173089, 31-201270 to S.G.). We gratefully acknowledge Michel Schaffhauser, Patrick Schlenker and Raymond Strittmatter (Biozentrum Central Mechanical Workshop) as well as Simon Saner (Biozentrum Central Electronics Workshop) for designing and building the xenon

pressure chamber apparatus, the Paul Scherrer Institut, Villigen, Switzerland for synchrotron radiation beamtime at beamline PXIII, the Biozentrum Biophysics Facility for access to their instruments, Dr. Jan Steyaert for the generous gift of the Nb80 plasmid, as well as Drs. Hans-Jürgen Sass, Chris Tate, Timm Maier, and Tilman Schirmer for helpful discussions.

AUTHOR CONTRIBUTIONS

L.A.A. and S.G. conceived the study. L.A.A. and A.G. expressed and purified protein and recorded NMR spectra. L.A.A. recorded high-pressure NMR experiments. L.A.A. analyzed and interpreted the NMR data. R.D.T. and S.E. recorded the X-ray data. R.D.T. analyzed the X-ray data. T.M. and T.S. performed and analyzed ITC experiments. L.A.A., R.D.T. and S.G. wrote the manuscript.

COMPETING INTERESTS STATEMENT

The authors declare no competing interests.

FIGURE LEGENDS

Figure 1. Xenon derivatization of TS-β_1AR. **a)** Pressure apparatus built for Xe derivatization with humidity control. The pressure chamber, wash bottle, humidity sensor and crystal loop are indicated. The insets show a close-up of the pressure chamber and a microscopic image of a β_1AR crystal during Xe pressurization. **b)** Left: Location of the two xenon binding sites (magenta surfaces) identified by anomalous X-ray scattering within the isoprenaline·β_1AR crystal structure (PDB 2y03). Isoprenaline is represented as gray sticks and CHS as orange spheres. Dashed green lines indicate the approximate membrane boundaries. Right: close-up of the Xe1 site, which colocalizes with the CHS molecule (orange sticks) of the crystal structure. **c)** Structure of the isoprenaline·β_1AR complex (PDB 2y03) and void volumes (shown as surfaces) determined with the program Hollow 1.2.54. Blue/yellow surfaces represent void volumes accessible/inaccessible to water, respectively. Xenon sites Xe1 and Xe2 are shown in magenta and CHS as orange sticks, respectively

Figure 2. High-pressure NMR analysis of agonist-bound β_1AR labeled by ^{15}N-valine in the presence or absence of CHS. a-c Superposition of ^{1}H-^{15}N TROSY

spectra of isoprenaline·YY-β_1AR with 1 mM CHS at 1 bar (black) and 2500 bar (red)(a), isoprenaline·YY-β_1AR without CHS at 1 bar (black) and 2500 bar (red) (b) and isoprenaline·YY-β_1AR with (orange) and without CHS (blue) at 2500 bar (c). Resonances are marked with assignment information. Resonances connected by a dashed magenta line represent residues with two clearly distinguishable resonances for the preactive ('p') and active ('a') conformations.

Figure 3. CHS shifts β_1AR from the active to the preactive conformation. **a)** Superposition of ^{1}H-^{15}N TROSY spectra of ^{15}N-valine-labeled YY-β_1AR with valine (YY-β_1AR) or isoleucine (YY-β_1AR-V129I) at position $129^{3.40}$ in the absence (black) or presence (orange) of 1 mM CHS at 1 bar. The valine resonances are marked with assignment information using the same color code as in panel **b)**. **b)** Valine residues represented as spheres in the crystal structures (PDB 2y03 - preactive, gray; PDB 6h7j - active, magenta) and colored according to their response to the addition of CHS (red: increase of the preactive conformation population; yellow: moderate chemical shift change; cyan: very small chemical shift change) for YY-β_1AR (left) and YY-β_1AR-V129I (right). **c)** Fraction of active-state population of YY-β_1AR (green) and YY-β_1AR-V129I (blue) in the absence and presence of CHS. Lower (+) and upper bounds (-) are indicated for cases where only one of the two resonances for the active or preactive conformation could be detected. In these cases, the bounds were derived from the assumption that the amplitude of the missing peak was smaller than three times the root-mean-square deviation of the spectral noise.

Figure 4. Effect of CHS on the thermodynamics of isoprenaline and Nb80 binding to YY-β_1AR-V129I. Exemple ITC isotherms for each set of experiments are shown for isoprenaline binding to the apo receptor (top) and Nb80 binding to the receptor in complex with isoprenaline (bottom), both in the absence (left) or presence (right) of CHS. The error bars correspond to the baseline uncertainty estimated as described in Keller et al.[83]. Globally fitted values from triplicate measurements for ΔH, ΔS, and K_D are indicated in the respective panels.

Figure 5. Structural basis of the allosteric inhibition of β_1AR by CHS. **a)** Comparison between preactive (PDB 2y03, gray) and active (PDB 6h7j, magenta) crystal structures. For clarity only two TMs are shown in each panel

together with their key interactions with CHS. Regions of steric clashes of CHS with the active conformation and attractive interactions with the inactive conformation are highlighted. Residues belonging to conserved GPCR microswitch motifs and affected by CHS are shown in varying colors (PIF, green; DRY, blue; NPxxY, brown). The direction of the activating motion is represented by magenta arrows. **b)** Schematic representation of the CHS-transmembrane helix interactions and direction of activating (magenta arrows) and inhibiting (orange arrows, induced by CHS) motions. **c)** Left: comparison of β_2AR structures in the active (PDB 4ldl, magenta) and preactive (PDB 6oba, gray) states with the negative modulator AS408 (cyan spheres). Right: comparison of agonist-bound MK-8666·GPR40 structures in the absence (PDB 5tzr, gray) and in the presence (PDB 5tzy, magenta) of the positive modulator AP8 (yellow spheres). For both receptors, only the parts of TM4 and TM5 close to the Xe1 binding site are shown together with key residues (spheres) interacting with the allosteric regulators. Receptor residues clashing with the ligand are indicated as dotted spheres. AS408 stabilizes the preactive conformation of TM5 in β_2AR, but would clash with its active conformation. By contrast, AP8 binding is incompatible with the preactive conformation of GPR40. As a result, the two allosteric modulators shift TM5 in the two receptors in opposite directions (magenta arrows indicate the direction of the activating TM5 motion, see text). **d)** Superposition of the isoprenaline·β_1AR (PDB 2y03, grey) and the BPTU·P2Y1R (PDB 4xnv, yellow) crystal structures in the vicinity of the β_1AR Xe1 and Xe2 sites (magenta surfaces). The allosteric antagonist BPTU (yellow) and CHS (orange) observed in the BPTU·P2Y1R structure are shown as sticks.

Figure 1.

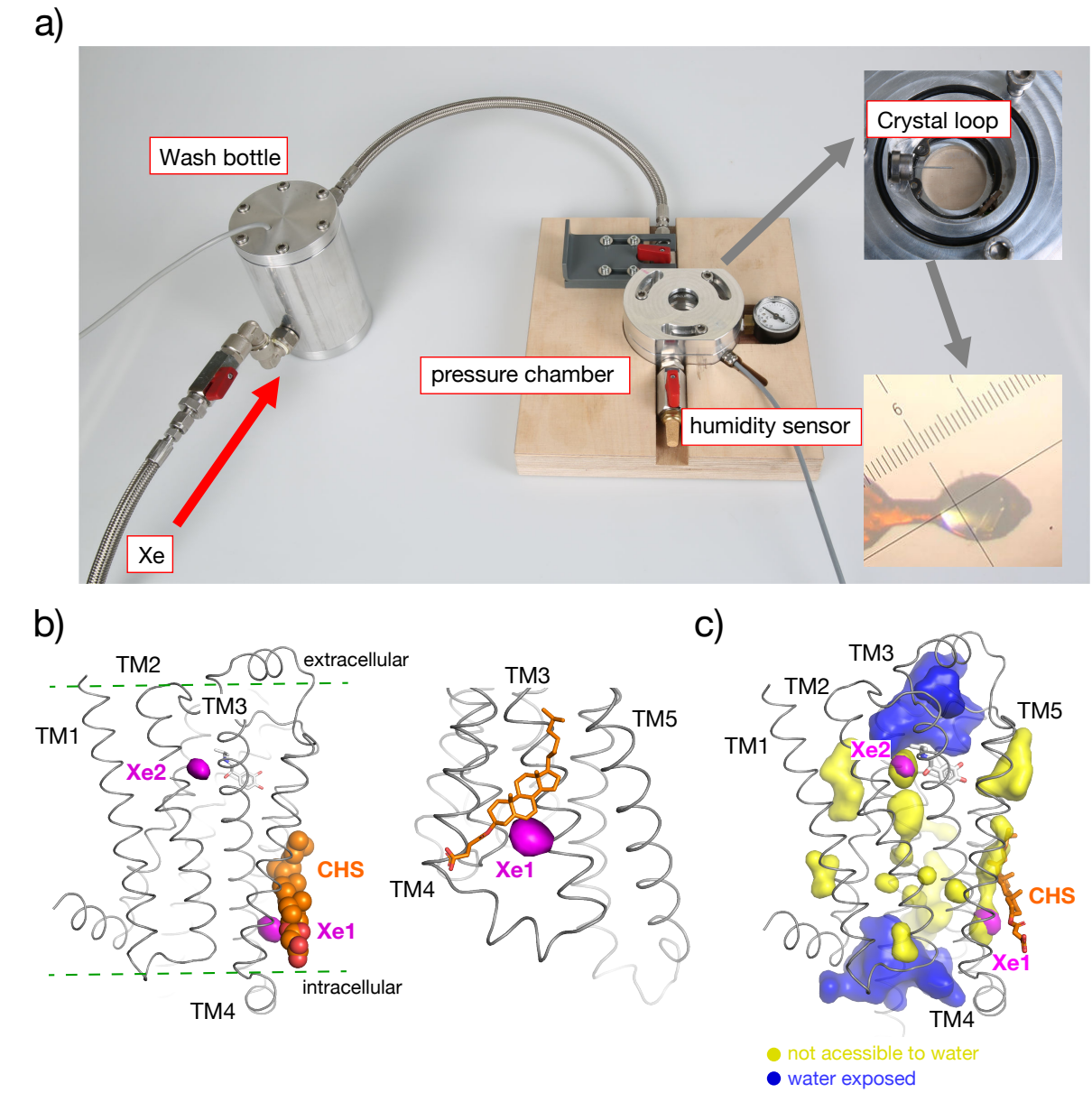

Figure 2.

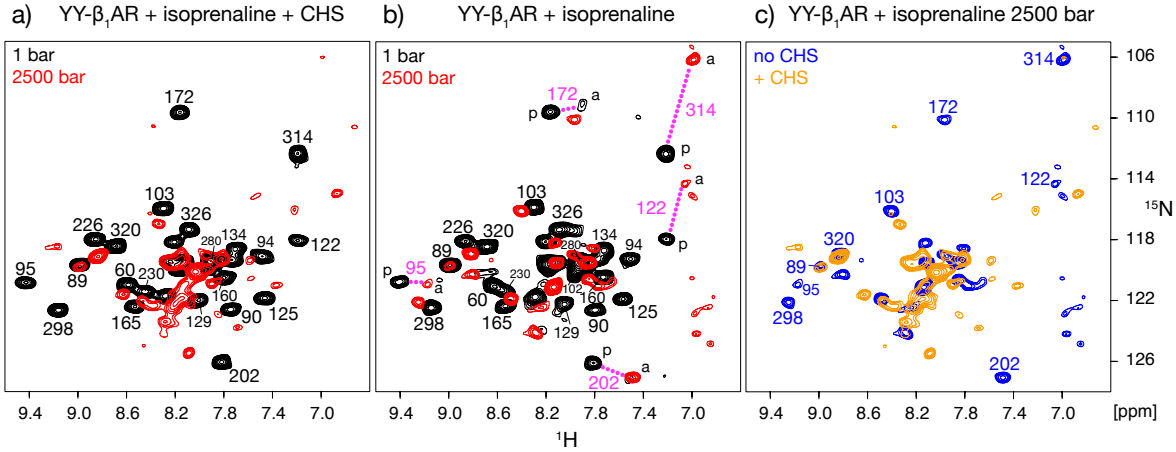

Figure 3.

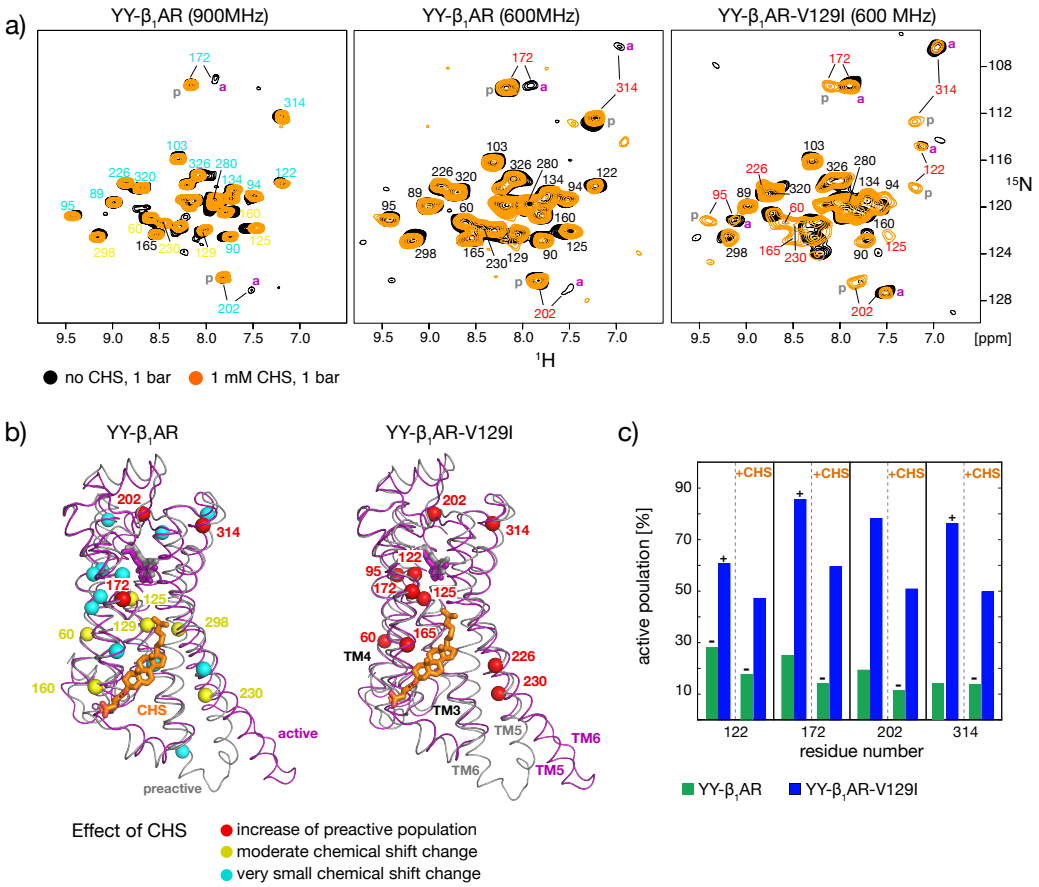

Figure 4.

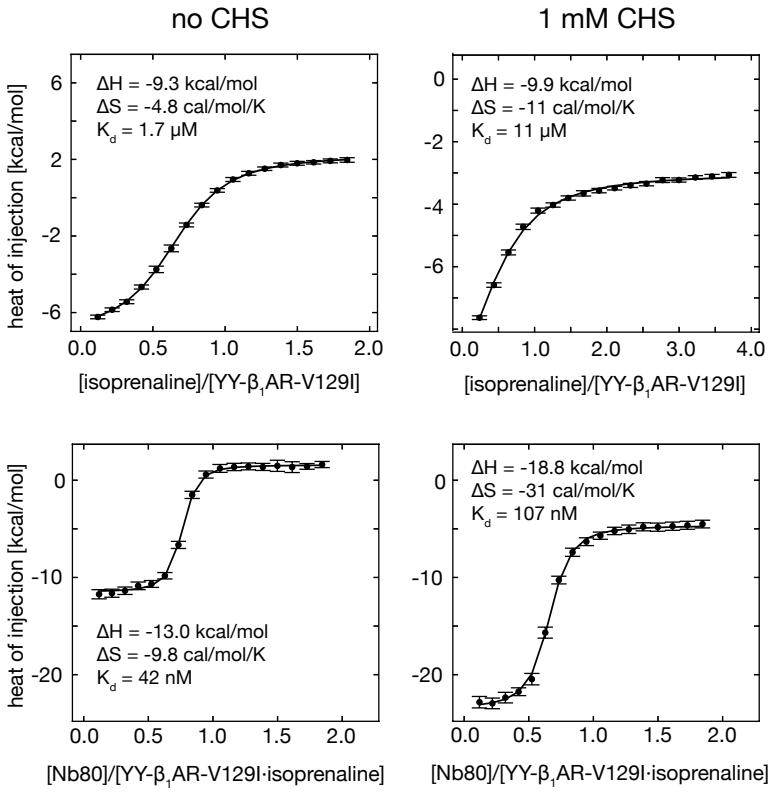

Figure 5.

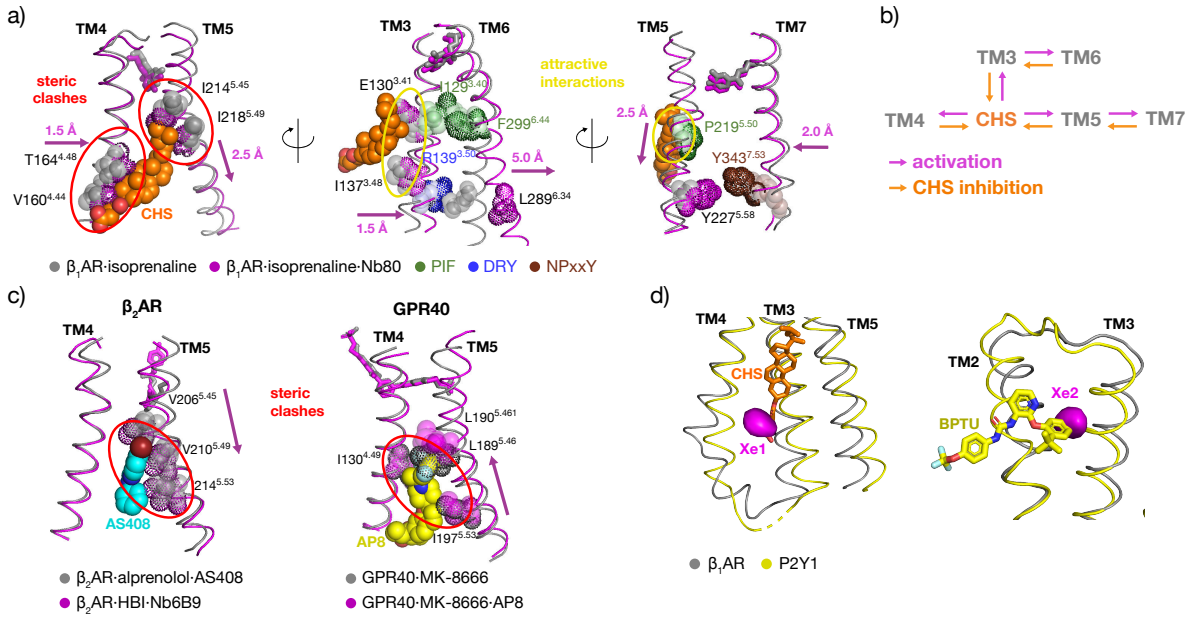
a)
TM4
TM5
steric clashes
I214^5.45
I218^5.49
1.5 Å
2.5 Å
T164^4.48
V160^4.44
CHS
TM3
TM6
E130^3.41
I129^3.40
F299^6.44
R139^3.50
5.0 Å
I137^3.48
L289^6.34
1.5 Å
attractive interactions
TM5
TM7
2.5 Å
2.0 Å
P219^5.50
Y343^7.53
Y227^5.58
β1AR·isoprenaline
β1AR·isoprenaline·Nb80
PIF
DRY
NPxxY
b)
TM3
TM6
TM4
CHS
TM5
TM7
activation
CHS inhibition
c)
β2AR
TM4
TM5
V206^5.45
V210^5.49
214^5.53
AS408
steric clashes
GPR40
TM4
TM5
L190^5.461
L189^5.46
I130^4.49
AP8
I197^5.53
β2AR·alprenolol·AS408
β2AR·HBI·Nb6B9
GPR40·MK-8666
GPR40·MK-8666·AP8
d)
TM4
TM3
TM5
CHS
Xe1
TM3
TM2
Xe2
BPTU
β1AR
P2Y1

REFERENCES

1. Hubbard, S. J., Gross, K.-H. & Argos, P. Intramolecular cavities in globular proteins. *Protein Engineering, Design and Selection* **7**, 613–626 (1994).
2. Williams, M. A., Goodfellow, J. M. & Thornton, J. M. Buried waters and internal cavities in monomeric proteins. *Protein Science* **3**, 1224–1235 (1994).
3. Otting, G., Liepinsh, E. & Wuthrich, K. Protein hydration in aqueous solution. *Science* **254**, 974–980 (1991).
4. Desvaux, H. *et al.* Dynamics of Xenon Binding Inside the Hydrophobic Cavity of Pseudo-Wild-type Bacteriophage T4 Lysozyme Explored through Xenon-Based NMR Spectroscopy. *J. Am. Chem. Soc.* **127**, 11676–11683 (2005).
5. Krimmer, S. G., Cramer, J., Schiebel, J., Heine, A. & Klebe, G. How Nothing Boosts Affinity: Hydrophobic Ligand Binding to the Virtually Vacated S1′ Pocket of Thermolysin. *J. Am. Chem. Soc.* **139**, 10419–10431 (2017).
6. Qvist, J., Davidovic, M., Hamelberg, D. & Halle, B. A dry ligand-binding cavity in a solvated protein. *Proc. Natl. Acad. Sci. USA* **105**, 6296–6301 (2008).
7. Otting, G., Liepinsh, E., Halle, B. & Frey, U. NMR identification of hydrophobic cavities with low water occupancies in protein structures using small gas molecules. *Nat Struct Mol Biol* **4**, 396–404 (1997).
8. Abiko, L. A., Grahl, A. & Grzesiek, S. High Pressure Shifts the β1-Adrenergic Receptor to the Active Conformation in the Absence of G Protein. *J. Am. Chem. Soc.* **141**, 16663–16670 (2019).
9. Alexander, S. P. *et al.* THE CONCISE GUIDE TO PHARMACOLOGY 2017/18: G protein-coupled receptors. *Br. J. Pharmacol.* **174 Suppl 1**, S17–S129 (2017).
10. Grahl, A., Abiko, L. A., Isogai, S., Sharpe, T. & Grzesiek, S. A high-resolution description of β1-adrenergic receptor functional dynamics and allosteric coupling from backbone NMR. *Nat. Commun.* **11**, 2216 (2020).
11. Isogai, S. *et al.* Backbone NMR reveals allosteric signal transduction networks in the β1-adrenergic receptor. *Nature* **530**, 237–241 (2016).
12. Kofuku, Y. *et al.* Efficacy of the β2-adrenergic receptor is determined by conformational equilibrium in the transmembrane region. *Nat. Commun.* **3**, 1045 (2012).
13. Latorraca, N. R., Venkatakrishnan, A. J. & Dror, R. O. GPCR Dynamics: Structures in Motion. *Chem. Rev.* **117**, 139–155 (2017).
14. Liu, J. J., Horst, R., Katritch, V., Stevens, R. C. & Wüthrich, K. Biased Signaling Pathways in β2-Adrenergic Receptor Characterized by 19F-NMR. *Science* **335**, 1106–1110 (2012).
15. Manglik, A. & Kobilka, B. The role of protein dynamics in GPCR function: insights from the β2AR and rhodopsin. *Curr. Opin. Cell Biol.* **27**, 136–143 (2014).
16. Okude, J. *et al.* Identification of a Conformational Equilibrium That Determines the Efficacy and Functional Selectivity of the μ-Opioid Receptor. *Angew. Chem. Int. Ed.* **54**, 15771–15776 (2015).
17. Venkatakrishnan, A. J. *et al.* Molecular signatures of G-protein-coupled receptors. *Nature* **494**, 185–194 (2013).
18. Ye, L., Van Eps, N., Zimmer, M., Ernst, O. P. & Scott Prosser, R. Activation of the A2A adenosine G-protein-coupled receptor by conformational selection. *Nature* **533**, 265–268 (2016).
19. Rasmussen, S. G. F. *et al.* Crystal structure of the β2 adrenergic receptor–Gs protein complex. *Nature* **477**, 549–555 (2011).

20. Ballesteros, J. A. & Weinstein, H. [19] Integrated methods for the construction of three-dimensional models and computational probing of structure-function relations in G protein-coupled receptors. in *Methods in Neurosciences* (ed. Sealfon, S. C.) vol. 25 366–428 (Academic Press, 1995).
21. Trzaskowski, B. *et al.* Action of molecular switches in GPCRs--theoretical and experimental studies. *Curr. Med. Chem.* **19**, 1090–1109 (2012).
22. Miller, J. L. & Tate, C. G. Engineering an Ultra-Thermostable β1-Adrenoceptor. *J. Mol. Biol.* **413**, 628–638 (2011).
23. Miller-Gallacher, J. L. *et al.* The 2.1 Å resolution structure of cyanopindolol-bound β1-adrenoceptor identifies an intramembrane Na+ ion that stabilises the ligand-free receptor. *PLoS One* **9**, e92727 (2014).
24. Heydenreich, F. M., Vuckovic, Z., Matkovic, M. & Veprintsev, D. B. Stabilization of G protein-coupled receptors by point mutations. *Front. Pharmacol.* **6**, (2015).
25. Warne, T. *et al.* Structure of a β1-adrenergic G-protein-coupled receptor. *Nature* **454**, 486–491 (2008).
26. Goncalves, J. A. *et al.* Highly conserved tyrosine stabilizes the active state of rhodopsin. *Proc. Natl. Acad. Sci. USA* **107**, 19861–19866 (2010).
27. Manglik, A. & Kruse, A. C. Structural Basis for G Protein-Coupled Receptor Activation. *Biochemistry* **56**, 5628–5634 (2017).
28. Oates, J. & Watts, A. Uncovering the intimate relationship between lipids, cholesterol and GPCR activation. *Curr. Opin. Struct. Biol.* **21**, 802–807 (2011).
29. Dawaliby, R. *et al.* Allosteric regulation of G protein–coupled receptor activity by phospholipids. *Nat. Chem. Biol.* **12**, 35–39 (2016).
30. Salas-Estrada, L. A., Leioatts, N., Romo, T. D. & Grossfield, A. Lipids Alter Rhodopsin Function via Ligand-like and Solvent-like Interactions. *Biophys. J.* **114**, 355–367 (2018).
31. Song, W., Yen, H.-Y., Robinson, C. V. & Sansom, M. S. P. State-dependent Lipid Interactions with the A2a Receptor Revealed by MD Simulations Using In Vivo-Mimetic Membranes. *Structure* **27**, 392-403.e3 (2019).
32. Duncan, A. L., Song, W. & Sansom, M. S. P. Lipid-Dependent Regulation of Ion Channels and G Protein–Coupled Receptors: Insights from Structures and Simulations. *Annu. Rev. Pharmacol. Toxicol.* **60**, 31–50 (2020).
33. Pucadyil, T. J. & Chattopadhyay, A. Role of cholesterol in the function and organization of G-protein coupled receptors. *Prog. Lipid Res.* **45**, 295–333 (2006).
34. Paila, Y. D. & Chattopadhyay, A. Membrane Cholesterol in the Function and Organization of G-Protein Coupled Receptors. in *Cholesterol Binding and Cholesterol Transport Proteins: Structure and Function in Health and Disease* (ed. Harris, J. R.) 439–466 (Springer Netherlands, 2010). doi:10.1007/978-90-481-8622-8_16.
35. Escribá, P. V. *et al.* Membrane lipid therapy: Modulation of the cell membrane composition and structure as a molecular base for drug discovery and new disease treatment. *Prog. Lipid Res.* **59**, 38–53 (2015).
36. Gimpl, G. Interaction of G protein coupled receptors and cholesterol. *Chem. Phys. Lipids* **199**, 61–73 (2016).
37. Jafurulla, Md., Aditya Kumar, G., Rao, B. D. & Chattopadhyay, A. A Critical Analysis of Molecular Mechanisms Underlying Membrane Cholesterol Sensitivity of GPCRs. in *Cholesterol Modulation of Protein Function: Sterol Specificity and Indirect Mechanisms* (eds. Rosenhouse-Dantsker, A. & Bukiya, A. N.) 21–52 (Springer International Publishing, 2019). doi:10.1007/978-3-030-04278-3_2.

38. Kiriakidi, S. *et al.* Effects of Cholesterol on GPCR Function: Insights from Computational and Experimental Studies. in *Direct Mechanisms in Cholesterol Modulation of Protein Function* (eds. Rosenhouse-Dantsker, A. & Bukiya, A. N.) 89–103 (Springer International Publishing, 2019). doi:10.1007/978-3-030-14265-0_5.
39. Casares, D., Escribá, P. V. & Rosselló, C. A. Membrane Lipid Composition: Effect on Membrane and Organelle Structure, Function and Compartmentalization and Therapeutic Avenues. *Int. J. Mol. Sci.* **20**, (2019).
40. Jakubík, J. & El-Fakahany, E. E. Allosteric Modulation of GPCRs of Class A by Cholesterol. *Int. J. Mol. Sci.* **22**, 1953 (2021).
41. Albert, A. D., Boesze-Battaglia, K., Paw, Z., Watts, A. & Epand, R. M. Effect of cholesterol on rhodopsin stability in disk membranes. *Biochim. Biophys. Acta (BBA) - Protein Structure and Molecular Enzymology* **1297**, 77–82 (1996).
42. Gimpl, G. & Fahrenholz, F. Cholesterol as stabilizer of the oxytocin receptor. *Biochimica et Biophysica Acta (BBA) - Biomembranes* **1564**, 384–392 (2002).
43. Yao, Z. & Kobilka, B. Using synthetic lipids to stabilize purified β2 adrenoceptor in detergent micelles. *Analytical Biochemistry* **343**, 344–346 (2005).
44. Jaakola, V.-P. *et al.* The 2.6 Angstrom Crystal Structure of a Human A2A Adenosine Receptor Bound to an Antagonist. *Science* **322**, 1211–1217 (2008).
45. Saxena, R. & Chattopadhyay, A. Membrane cholesterol stabilizes the human serotonin1A receptor. *Biochim. Biophys. Acta (BBA) - Biomembranes* **1818**, 2936–2942 (2012).
46. Zocher, M., Zhang, C., Rasmussen, S. G. F., Kobilka, B. K. & Müller, D. J. Cholesterol increases kinetic, energetic, and mechanical stability of the human β2-adrenergic receptor. *Proc. Natl. Acad. Sci. USA* **109**, E3463–E3472 (2012).
47. Abiko, L. A., Rogowski, M., Gautier, A., Schertler, G. & Grzesiek, S. Efficient production of a functional G protein-coupled receptor in E. coli for structural studies. *J. Biomol. NMR* **75**, 25–38 (2021).
48. Bari, M., Paradisi, A., Pasquariello, N. & Maccarrone, M. Cholesterol-dependent modulation of type 1 cannabinoid receptors in nerve cells. *J. Neurosci. Res.* **81**, 275–283 (2005).
49. Harikumar, K. G. *et al.* Differential Effects of Modification of Membrane Cholesterol and Sphingolipids on the Conformation, Function, and Trafficking of the G Protein-coupled Cholecystokinin Receptor*. *J. Biol. Chem.* **280**, 2176–2185 (2005).
50. Muth, S., Fries, A. & Gimpl, G. Cholesterol-induced conformational changes in the oxytocin receptor. *Biochem. J.* **437**, 541–553 (2011).
51. Qiu, Y., Wang, Y., Law, P.-Y., Chen, H.-Z. & Loh, H. H. Cholesterol Regulates μ-Opioid Receptor-Induced β-Arrestin 2 Translocation to Membrane Lipid Rafts. *Mol. Pharmacol.* **80**, 210–218 (2011).
52. Casiraghi, M. *et al.* Functional Modulation of a G Protein-Coupled Receptor Conformational Landscape in a Lipid Bilayer. *J. Am. Chem. Soc.* **138**, 11170–11175 (2016).
53. Manna, M. *et al.* Mechanism of allosteric regulation of β2-adrenergic receptor by cholesterol. *eLife* **5**, e18432 (2016).
54. Hanson, M. A. *et al.* A Specific Cholesterol Binding Site Is Established by the 2.8 Å Structure of the Human β2-Adrenergic Receptor. *Structure* **16**, 897–905 (2008).
55. Liu, W. *et al.* Structural Basis for Allosteric Regulation of GPCRs by Sodium Ions. *Science* **337**, 232–236 (2012).

56. Wacker, D. *et al.* Structural Features for Functional Selectivity at Serotonin Receptors. *Science* **340**, 615–619 (2013).
57. Manglik, A. *et al.* Crystal structure of the μ-opioid receptor bound to a morphinan antagonist. *Nature* **485**, 321–326 (2012).
58. Zhang, K. *et al.* Structure of the human P2Y12 receptor in complex with an antithrombotic drug. *Nature* **509**, 115–118 (2014).
59. Wu, H. *et al.* Structure of a class C GPCR metabotropic glutamate receptor 1 bound to an allosteric modulator. *Science* **344**, 58–64 (2014).
60. Burg, J. S. *et al.* Structural biology. Structural basis for chemokine recognition and activation of a viral G protein-coupled receptor. *Science* **347**, 1113–1117 (2015).
61. Taghon, G. J., Rowe, J. B., Kapolka, N. J. & Isom, D. G. Predictable cholesterol binding sites in GPCRs lack consensus motifs. *Structure* **29**, 499-506.e3 (2021).
62. Huang, S. K. *et al.* Allosteric modulation of the adenosine A2A receptor by cholesterol. *eLife* **11**, e73901 (2022).
63. Li, L. B., Vorobyov, I. & Allen, T. W. The role of membrane thickness in charged protein–lipid interactions. *Biochim. Biophys. Acta (BBA) - Biomembranes* **1818**, 135–145 (2012).
64. Mondal, S. *et al.* Membrane Driven Spatial Organization of GPCRs. *Sci. Rep.* **3**, 2909 (2013).
65. Róg, T. & Vattulainen, I. Cholesterol, sphingolipids, and glycolipids: What do we know about their role in raft-like membranes? *Chem. Phys. Lipids* **184**, 82–104 (2014).
66. Kulig, W. *et al.* How well does cholesteryl hemisuccinate mimic cholesterol in saturated phospholipid bilayers? *J. Mol. Model.* **20**, 2121 (2014).
67. Warne, T. *et al.* The structural basis for agonist and partial agonist action on a β1-adrenergic receptor. *Nature* **469**, 241–244 (2011).
68. Cang, X. *et al.* Cholesterol-β1AR interaction versus cholesterol-β2AR interaction. *Proteins: Structure, Function, and Bioinformatics* **82**, 760–770 (2014).
69. Quillin, M. L., Breyer, W. A., Griswold, I. J. & Matthews, B. W. Size versus polarizability in protein-ligand interactions: binding of noble gases within engineered cavities in phage T4 lysozyme11Edited by B. Honig. *J. Mol. Biol.* **302**, 955–977 (2000).
70. Guixà-González, R. *et al.* Membrane cholesterol access into a G-protein-coupled receptor. *Nat. Commun.* **8**, 14505 (2017).
71. Warne, T., Edwards, P. C., Doré, A. S., Leslie, A. G. W. & Tate, C. G. Molecular basis for high-affinity agonist binding in GPCRs. *Science* **364**, 775 (2019).
72. Liu, X. *et al.* An allosteric modulator binds to a conformational hub in the β2 adrenergic receptor. *Nat. Chem. Biol.* **16**, 749–755 (2020).
73. Lu, J. *et al.* Structural basis for the cooperative allosteric activation of the free fatty acid receptor GPR40. *Nat. Struct. Mol. Biol.* **24**, 570–577 (2017).
74. Zhang, D. *et al.* Two disparate ligand-binding sites in the human P2Y1 receptor. *Nature* **520**, 317–321 (2015).
75. Vial, C., Fung, C. Y. E., Goodall, A. H., Mahaut-Smith, M. P. & Evans, R. J. Differential sensitivity of human platelet P2X1 and P2Y1 receptors to disruption of lipid rafts. *Biochem. Biophys. Res. Commun.* **343**, 415–419 (2006).
76. Prangé, T. *et al.* Exploring hydrophobic sites in proteins with xenon or krypton. *Proteins: Structure, Function, and Bioinformatics* **30**, 61–73 (1998).

77. Paila, Y. D., Jindal, E., Goswami, S. K. & Chattopadhyay, A. Cholesterol depletion enhances adrenergic signaling in cardiac myocytes. *Biochim. Biophys. Acta (BBA) - Biomembranes* **1808**, 461–465 (2011).
78. Yeliseev, A. *et al.* Cholesterol as a modulator of cannabinoid receptor CB2 signaling. *Sci. Rep.* **11**, 3706 (2021).
79. Xiao, P. *et al.* Ligand recognition and allosteric regulation of DRD1-Gs signaling complexes. *Cell* **184**, 943-956.e18 (2021).
80. Robertson, N. *et al.* Structure of the complement C5a receptor bound to the extra-helical antagonist NDT9513727. *Nature* **553**, 111–114 (2018).
81. Cheng, R. K. Y. *et al.* Structural insight into allosteric modulation of protease-activated receptor 2. *Nature* **545**, 112–115 (2017).
82. Thal, D. M., Glukhova, A., Sexton, P. M. & Christopoulos, A. Structural insights into G-protein-coupled receptor allostery. *Nature* **559**, 45–53 (2018).
83. Keller, S. *et al.* High-Precision Isothermal Titration Calorimetry with Automated Peak-Shape Analysis. *Anal. Chem.* **84**, 5066–5073 (2012).
84. Rasmussen, S. G. F. *et al.* Structure of a nanobody-stabilized active state of the β2 adrenoceptor. *Nature* **469**, 175–180 (2011).
85. Warne, T., Serrano-Vega, M. J., Tate, C. G. & Schertler, G. F. X. Development and crystallization of a minimal thermostabilised G protein-coupled receptor. *Protein Expr. Purif.* **65**, 204–213 (2009).
86. McCoy, A. J. *et al.* Phaser crystallographic software. *J. Appl. Cryst.* **40**, 658–674 (2007).
87. Winn, M. D. *et al.* Overview of the CCP4 suite and current developments. *Acta Cryst. D* **67**, 235–242 (2011).
88. Vonrhein, C. *et al.* Data processing and analysis with the autoPROC toolbox. *Acta Cryst. D* **67**, 293–302 (2011).
89. Kabsch, W. XDS. *Acta Crystallogr. D Biol. Crystallogr.* **66**, 125–132 (2010).
90. Sheldrick, G. M. Experimental phasing with SHELXC/D/E: combining chain tracing with density modification. *Acta Cryst. D* **66**, 479–485 (2010).
91. Thorn, A. & Sheldrick, G. M. ANODE: anomalous and heavy-atom density calculation. *J. Appl. Crystallogr.* **44**, 1285–1287 (2011).
92. Liebschner, D. *et al.* Macromolecular structure determination using X-rays, neutrons and electrons: recent developments in Phenix. *Acta Cryst D* **75**, 861–877 (2019).
93. Schrödinger, LLC. The PyMOL Molecular Graphics System, Version 1.8. (2015).
94. Ho, B. K. & Gruswitz, F. HOLLOW: Generating Accurate Representations of Channel and Interior Surfaces in Molecular Structures. *BMC Struct. Biol.* **8**, 49 (2008).
95. Sklenář, V. & Bax, A. Spin-echo water suppression for the generation of pure-phase two-dimensional NMR spectra. *J. Magn. Reson.* **74**, 469–479 (1987).
96. Scheuermann, T. H. & Brautigam, C. A. High-precision, automated integration of multiple isothermal titration calorimetric thermograms: new features of NITPIC. *Methods* **76**, 87–98 (2015).
97. Zhao, H., Piszczek, G. & Schuck, P. SEDPHAT--a platform for global ITC analysis and global multi-method analysis of molecular interactions. *Methods* **76**, 137–148 (2015).
98. Brautigam, C. A. Calculations and Publication-Quality Illustrations for Analytical Ultracentrifugation Data. *Methods Enzymol.* **562**, 109–133 (2015).

METHODS

Protein expression and purification

Expression of the unlabelled, thermostabilized turkey β_1AR construct (TS-β_1AR), as well as of ^{15}N-valine-labelled G protein binding-competent construct (YY-β_1AR) in baculovirus-infected Sf9 cells, purification, assignments, binding of ligands, and exchange between ligands were carried out as described previously[11]. The Nb80 protein was expressed in *Escherichia coli* and purified according to the described procedure[84].

For the TS-β_1AR crystallization sample, an additional size-exclusion purification step was added to increase the sample homogeneity and to exchange the detergent from decylmaltoside (DM) to Hega-10. For this, ~900 µL of 100 µM TS-β_1AR was applied at 0.3 mL/min to a 24-mL Superdex 200 Increase 10/300 GL column (GE healthcare) pre-equilibrated with 10 mM Tris-HCl, 100 mM NaCl, 0.1 mM EDTA, 1 mM isoprenaline, 0.35% Hega-10, pH 7.5. The receptor was eluted at 0.3 mL/min with the same buffer, and concentrated with a 50-kDa molecular weight cutoff centrifugal filter (Amicon) to a final concentration of ~10–15 mg/mL.

Crystallization

The crystallization of the isoprenaline·TS-β_1AR complex was performed following the protocol established by Tate and coworkers[67] using CHS as an additive. The addition of CHS improves the quality of the crystals, presumably due to the increase of receptor rigidity and stability. In brief, immediately before setting up the crystallization plates, CHS was added to the isoprenaline·TS-β_1AR complex to a final concentration of 0.45 mg/mL (from a 10 mg/mL stock solution in 2% Hega-10). The receptor solution was subsequently centrifuged at 130'000 g through a 0.22-µm Ultrafree-MC spin filter (Millipore) for 5 min at 4˚C in order to remove possible aggregates. Crystals were grown under similar conditions as described previously[67,85] on MRC Maxi 48-well crystallization plates (Swissci) by vapor diffusion in sitting drops containing 1 µL of protein solution + 1 µL of reservoir solutions consisting of 0.1 M Tris-HCl (pH 7.5–9.0), and 20–30% PEG 600. Plates were incubated at 4 ˚C until crystals reached their maximum size

after ~2 weeks. Typically, the obtained crystals were rod-shaped with dimensions of ~250x75x30 μm^3.

Xenon derivatization

Xenon derivatization of the isoprenaline·TS-β_1AR crystals was not possible with the commonly used commercial Xcell (Oxford Cryosystems), since the fragile GPCR crystals dried and broke after a few minutes of pressurization. For this reason, we built a pressure cell equipped with a wash bottle for humidity equilibration as prechamber and a humidity sensor, in which the humidity can be adjusted to arbitrary values using suitable aqueous salt solutions in the wash bottle. A relative humidity of 100% produced by pure water proved suitable to maintain TS-β_1AR crystals stable for long periods without changes in their appearance. After the xenon incubation, the xenon pressure was released and the crystals were flash-frozen in liquid nitrogen within seconds. Derivatization conditions were varied between 5–30 min incubation and 5–12 bar xenon pressure at 4 °C. The strongest anomalous signal was obtained for crystals incubated for 20 minutes at a xenon pressure of 5 bar. Cryoprotectant soaking with PEG 600 before crystal incubation with xenon did not improve crystal quality.

Data collection and structure determination

X-ray diffraction data were collected at the Swiss Light Source, Paul Scherrer Institute (Villigen, Switzerland), using the PXIII beamline equipped with a PILATUS 2MF detector (Dectris, Baden-Dättwil, Switzerland). Isoprenaline·TS-β_1AR crystals belonged to the space group $P2_1$ with the following unit cell parameters a=59.324 Å, b=125.653 Å, c=87.774 Å and β=104.76°. The crystal structure was solved by molecular replacement using the atomic coordinates of the β_1AR from PDB entry 2y03 (chain A) as a template, and searching for two β_1AR molecules using the program PHASER[86] contained in the CCP4i2 (version 1.0.2) package[87]. In order to maximize the anomalous contribution of the Xe atoms, diffraction data were recorded at 6.0 keV on four different crystals under varying *chi* angles. The individual *chi*-angle data sets were then processed using the autoPROC pipeline[88] and merged for each crystal with XSCALE[89]. Identification of Xe atoms was performed by computing Fourier maps using

SHELXC[90] and ANODE[91]. The two xenon binding sites (Xe1 and Xe2) described in the manuscript correspond to the strongest anomalous signals detected in all four crystals and present in both chains (A and B) of the asymmetric unit (Supplementary Table S2). Individual Xe occupancies were refined using PHENIX.REFINE[92] yielding values of 15 and 18% for Xe1 and Xe2, respectively. The anomalous peak heights of the two additional Xe atoms were too low for refinement. This suggest occupancies of 10% or less for these 2 atoms.

Analysis of crystal structures

All molecular representations were generated using the PyMOL 2.1. Molecular Graphics System[93]. The various receptor structures were aligned on the following TM regions: 1.46–1.51, 2.46–2.56, 3.34–3.44, 4.48–4.56, 7.38–7.46. Voids in the crystal structure of isoprenaline·β_1AR (PDB 2y03) were identified and quantified using the program Hollow 1.2.[94] as described previously[8] using a grid spacing of 1.0 Å and a sphere size of 4 Å for defining the receptor surface. Water and detergent molecules (including CHS) were removed before the analysis.

NMR experiments

NMR samples were prepared with typical receptor concentrations of 100−200 µM in 20 mM Tris-HCl, 100 mM NaCl, ~40 mM DM, 0.02% NaN_3, 5% D_2O (10% for high-pressure experiments), pH 7.5. The isoprenaline·β_1AR complex was formed by adding 2 mM isoprenaline and 20 mM sodium ascorbate (to prevent oxidation of the ligand) to the apo receptor. For formation of the ternary complex, a 1.2-molar equivalent of Nb80 was added to the isoprenaline·β_1AR complex. For measurements in the presence of 1 or 2 mM CHS, suitable volumes of 10 mg/mL CHS stock solution in 20 mM Tris-HCl pH 7.5, 100 mM NaCl, 0.1 % DM were added directly to the NMR sample.

The ^{1}H-^{15}N TROSY NMR experiments were recorded on Bruker AVANCE 900 MHz or AVANCE 600 MHz spectrometers equipped with TCI cryoprobes at 304 K using sample volumes of ~250 µL either in Shigemi microtubes or a commercial high-pressure NMR cell (3 mm inner diameter, 120 µl active volume, rated to 2,500 bar, Daedalus Innovations LLC) as described previously[8]. The

sample stability during longer NMR experiments was monitored by interleaved, one-dimensional ^{1}H experiments with spin-echo water suppression[95].

ITC experiments

For ITC measurements 400-µL volumes of 200 µM YY-β_1AR-V129I and 1.8 mM Nb80 were dialyzed overnight at 4 ˚C in Slide-A-Lyzer cassettes (Millipore; MWCO 20 kDa for YY-β_1AR-V129I, 3 kDa for Nb80) against 500 mL ITC buffer (20 mM Tris-HCl, 100 mM NaCl, 0.1% DM, pH 7.5). Dialyzed samples were diluted with ITC buffer to volumes of 500 µL yielding final concentrations of 140 µM YY-β_1AR-V129I and 480 µM Nb80.

For experiments in the presence of CHS a clear CHS stock solution of 1 mg/mL CHS and 0.1% DM in ITC buffer was prepared by stirring at 80 ˚C, followed by ultrasonication. This CHS stock solution was then added to both ITC cell and syringe samples to yield final concentrations of 1 mM CHS. Ascorbic acid was added to all samples containing isoprenaline (twice its molarity) to prevent oxidation. Samples were then incubated overnight at the same temperature as the ITC measurements, followed by an additional 30-min equilibration inside the equipment prior to measurement.

ITC data were collected with an ITC200 instrument (Malvern Panalytical) at 750 rpm stirring speed and high gain with 19 2-µL injections at 180-sec interval at 25 °C for receptor complexes with isoprenaline and 20 °C for the apo receptor, due to its lower stability. Titrations were performed as follows: 1) 100 µM Nb80 titrated into 10 µM YY-β_1AR-V129I and 500 µM (-)-isomer of isoprenaline, in the presence or absence of 1 mM CHS, 2) 300 µM (-)-isoprenaline was titrated into 30 µM apo YY-β_1AR-V129I, and 3) 600 µM (-)-isoprenaline was titrated into 30 µM apo YY-β_1AR-V129I in the presence of 1 mM CHS. All titrations were conducted in triplicate except for 3) and controls were in the absence of receptor (Supplementary Fig. 5).

The data were integrated using NITPIC[96] and fitted globally using a 1:1 model enabling correction for inactive receptor with SEDPHAT[97]. The ITC figures were prepared using GUSSI[98].

DATA AVAILABILITY

NMR spectra, ITC raw data, as well as structure factors, phases and density maps derived from the anomalous scattering data of the four xenon-derivatized isoprenaline·β_1AR crystals and the β_1AR structure derived from the first crystal have been deposited in the Zenodo repository under DOI 10.5281/zenodo.4926013.

REFERENCES

1. Hubbard, S. J., Gross, K.-H. & Argos, P. Intramolecular cavities in globular proteins. *Protein Engineering, Design and Selection* **7**, 613–626 (1994).
2. Williams, M. A., Goodfellow, J. M. & Thornton, J. M. Buried waters and internal cavities in monomeric proteins. *Protein Science* **3**, 1224–1235 (1994).
3. Otting, G., Liepinsh, E. & Wuthrich, K. Protein hydration in aqueous solution. *Science* **254**, 974–980 (1991).
4. Desvaux, H. *et al.* Dynamics of Xenon Binding Inside the Hydrophobic Cavity of Pseudo-Wild-type Bacteriophage T4 Lysozyme Explored through Xenon-Based NMR Spectroscopy. *J. Am. Chem. Soc.* **127**, 11676–11683 (2005).
5. Krimmer, S. G., Cramer, J., Schiebel, J., Heine, A. & Klebe, G. How Nothing Boosts Affinity: Hydrophobic Ligand Binding to the Virtually Vacated S1′ Pocket of Thermolysin. *J. Am. Chem. Soc.* **139**, 10419–10431 (2017).
6. Qvist, J., Davidovic, M., Hamelberg, D. & Halle, B. A dry ligand-binding cavity in a solvated protein. *Proc. Natl. Acad. Sci. USA* **105**, 6296–6301 (2008).
7. Otting, G., Liepinsh, E., Halle, B. & Frey, U. NMR identification of hydrophobic cavities with low water occupancies in protein structures using small gas molecules. *Nat Struct Mol Biol* **4**, 396–404 (1997).
8. Abiko, L. A., Grahl, A. & Grzesiek, S. High Pressure Shifts the β1-Adrenergic Receptor to the Active Conformation in the Absence of G Protein. *J. Am. Chem. Soc.* **141**, 16663–16670 (2019).
9. Alexander, S. P. *et al.* THE CONCISE GUIDE TO PHARMACOLOGY 2017/18: G protein-coupled receptors. *Br. J. Pharmacol.* **174 Suppl 1**, S17–S129 (2017).
10. Grahl, A., Abiko, L. A., Isogai, S., Sharpe, T. & Grzesiek, S. A high-resolution description of β1-adrenergic receptor functional dynamics and allosteric coupling from backbone NMR. *Nat. Commun.* **11**, 2216 (2020).
11. Isogai, S. *et al.* Backbone NMR reveals allosteric signal transduction networks in the β1-adrenergic receptor. *Nature* **530**, 237–241 (2016).
12. Kofuku, Y. *et al.* Efficacy of the β2-adrenergic receptor is determined by conformational equilibrium in the transmembrane region. *Nat. Commun.* **3**, 1045 (2012).
13. Latorraca, N. R., Venkatakrishnan, A. J. & Dror, R. O. GPCR Dynamics: Structures in Motion. *Chem. Rev.* **117**, 139–155 (2017).

14. Liu, J. J., Horst, R., Katritch, V., Stevens, R. C. & Wüthrich, K. Biased Signaling Pathways in β2-Adrenergic Receptor Characterized by 19F-NMR. *Science* **335**, 1106–1110 (2012).
15. Manglik, A. & Kobilka, B. The role of protein dynamics in GPCR function: insights from the β2AR and rhodopsin. *Curr. Opin. Cell Biol.* **27**, 136–143 (2014).
16. Okude, J. *et al.* Identification of a Conformational Equilibrium That Determines the Efficacy and Functional Selectivity of the μ-Opioid Receptor. *Angew. Chem. Int. Ed.* **54**, 15771–15776 (2015).
17. Venkatakrishnan, A. J. *et al.* Molecular signatures of G-protein-coupled receptors. *Nature* **494**, 185–194 (2013).
18. Ye, L., Van Eps, N., Zimmer, M., Ernst, O. P. & Scott Prosser, R. Activation of the A2A adenosine G-protein-coupled receptor by conformational selection. *Nature* **533**, 265–268 (2016).
19. Rasmussen, S. G. F. *et al.* Crystal structure of the β2 adrenergic receptor–Gs protein complex. *Nature* **477**, 549–555 (2011).
20. Ballesteros, J. A. & Weinstein, H. [19] Integrated methods for the construction of three-dimensional models and computational probing of structure-function relations in G protein-coupled receptors. in *Methods in Neurosciences* (ed. Sealfon, S. C.) vol. 25 366–428 (Academic Press, 1995).
21. Trzaskowski, B. *et al.* Action of molecular switches in GPCRs--theoretical and experimental studies. *Curr. Med. Chem.* **19**, 1090–1109 (2012).
22. Miller, J. L. & Tate, C. G. Engineering an Ultra-Thermostable β1-Adrenoceptor. *J. Mol. Biol.* **413**, 628–638 (2011).
23. Miller-Gallacher, J. L. *et al.* The 2.1 Å resolution structure of cyanopindolol-bound β1-adrenoceptor identifies an intramembrane Na+ ion that stabilises the ligand-free receptor. *PLoS One* **9**, e92727 (2014).
24. Heydenreich, F. M., Vuckovic, Z., Matkovic, M. & Veprintsev, D. B. Stabilization of G protein-coupled receptors by point mutations. *Front. Pharmacol.* **6**, (2015).
25. Warne, T. *et al.* Structure of a β1-adrenergic G-protein-coupled receptor. *Nature* **454**, 486–491 (2008).
26. Goncalves, J. A. *et al.* Highly conserved tyrosine stabilizes the active state of rhodopsin. *Proc. Natl. Acad. Sci. USA* **107**, 19861–19866 (2010).
27. Manglik, A. & Kruse, A. C. Structural Basis for G Protein-Coupled Receptor Activation. *Biochemistry* **56**, 5628–5634 (2017).
28. Oates, J. & Watts, A. Uncovering the intimate relationship between lipids, cholesterol and GPCR activation. *Curr. Opin. Struct. Biol.* **21**, 802–807 (2011).
29. Dawaliby, R. *et al.* Allosteric regulation of G protein–coupled receptor activity by phospholipids. *Nat. Chem. Biol.* **12**, 35–39 (2016).
30. Salas-Estrada, L. A., Leioatts, N., Romo, T. D. & Grossfield, A. Lipids Alter Rhodopsin Function via Ligand-like and Solvent-like Interactions. *Biophys. J.* **114**, 355–367 (2018).

31. Song, W., Yen, H.-Y., Robinson, C. V. & Sansom, M. S. P. State-dependent Lipid Interactions with the A2a Receptor Revealed by MD Simulations Using In Vivo-Mimetic Membranes. *Structure* **27**, 392-403.e3 (2019).
32. Duncan, A. L., Song, W. & Sansom, M. S. P. Lipid-Dependent Regulation of Ion Channels and G Protein–Coupled Receptors: Insights from Structures and Simulations. *Annu. Rev. Pharmacol. Toxicol.* **60**, 31–50 (2020).
33. Pucadyil, T. J. & Chattopadhyay, A. Role of cholesterol in the function and organization of G-protein coupled receptors. *Prog. Lipid Res.* **45**, 295–333 (2006).
34. Paila, Y. D. & Chattopadhyay, A. Membrane Cholesterol in the Function and Organization of G-Protein Coupled Receptors. in *Cholesterol Binding and Cholesterol Transport Proteins: Structure and Function in Health and Disease* (ed. Harris, J. R.) 439–466 (Springer Netherlands, 2010). doi:10.1007/978-90-481-8622-8_16.
35. Escribá, P. V. *et al.* Membrane lipid therapy: Modulation of the cell membrane composition and structure as a molecular base for drug discovery and new disease treatment. *Prog. Lipid Res.* **59**, 38–53 (2015).
36. Gimpl, G. Interaction of G protein coupled receptors and cholesterol. *Chem. Phys. Lipids* **199**, 61–73 (2016).
37. Jafurulla, Md., Aditya Kumar, G., Rao, B. D. & Chattopadhyay, A. A Critical Analysis of Molecular Mechanisms Underlying Membrane Cholesterol Sensitivity of GPCRs. in *Cholesterol Modulation of Protein Function: Sterol Specificity and Indirect Mechanisms* (eds. Rosenhouse-Dantsker, A. & Bukiya, A. N.) 21–52 (Springer International Publishing, 2019). doi:10.1007/978-3-030-04278-3_2.
38. Kiriakidi, S. *et al.* Effects of Cholesterol on GPCR Function: Insights from Computational and Experimental Studies. in *Direct Mechanisms in Cholesterol Modulation of Protein Function* (eds. Rosenhouse-Dantsker, A. & Bukiya, A. N.) 89–103 (Springer International Publishing, 2019). doi:10.1007/978-3-030-14265-0_5.
39. Casares, D., Escribá, P. V. & Rosselló, C. A. Membrane Lipid Composition: Effect on Membrane and Organelle Structure, Function and Compartmentalization and Therapeutic Avenues. *Int. J. Mol. Sci.* **20**, (2019).
40. Jakubík, J. & El-Fakahany, E. E. Allosteric Modulation of GPCRs of Class A by Cholesterol. *Int. J. Mol. Sci.* **22**, 1953 (2021).
41. Albert, A. D., Boesze-Battaglia, K., Paw, Z., Watts, A. & Epand, R. M. Effect of cholesterol on rhodopsin stability in disk membranes. *Biochim. Biophys. Acta (BBA) - Protein Structure and Molecular Enzymology* **1297**, 77–82 (1996).
42. Gimpl, G. & Fahrenholz, F. Cholesterol as stabilizer of the oxytocin receptor. *Biochimica et Biophysica Acta (BBA) - Biomembranes* **1564**, 384–392 (2002).
43. Yao, Z. & Kobilka, B. Using synthetic lipids to stabilize purified β2 adrenoceptor in detergent micelles. *Analytical Biochemistry* **343**, 344–346 (2005).

44. Jaakola, V.-P. *et al.* The 2.6 Angstrom Crystal Structure of a Human A2A Adenosine Receptor Bound to an Antagonist. *Science* **322**, 1211–1217 (2008).
45. Saxena, R. & Chattopadhyay, A. Membrane cholesterol stabilizes the human serotonin1A receptor. *Biochim. Biophys. Acta (BBA) - Biomembranes* **1818**, 2936–2942 (2012).
46. Zocher, M., Zhang, C., Rasmussen, S. G. F., Kobilka, B. K. & Müller, D. J. Cholesterol increases kinetic, energetic, and mechanical stability of the human β2-adrenergic receptor. *Proc. Natl. Acad. Sci. USA* **109**, E3463–E3472 (2012).
47. Abiko, L. A., Rogowski, M., Gautier, A., Schertler, G. & Grzesiek, S. Efficient production of a functional G protein-coupled receptor in E. coli for structural studies. *J. Biomol. NMR* **75**, 25–38 (2021).
48. Bari, M., Paradisi, A., Pasquariello, N. & Maccarrone, M. Cholesterol-dependent modulation of type 1 cannabinoid receptors in nerve cells. *J. Neurosci. Res.* **81**, 275–283 (2005).
49. Harikumar, K. G. *et al.* Differential Effects of Modification of Membrane Cholesterol and Sphingolipids on the Conformation, Function, and Trafficking of the G Protein-coupled Cholecystokinin Receptor*. *J. Biol. Chem.* **280**, 2176–2185 (2005).
50. Muth, S., Fries, A. & Gimpl, G. Cholesterol-induced conformational changes in the oxytocin receptor. *Biochem. J.* **437**, 541–553 (2011).
51. Qiu, Y., Wang, Y., Law, P.-Y., Chen, H.-Z. & Loh, H. H. Cholesterol Regulates μ-Opioid Receptor-Induced β-Arrestin 2 Translocation to Membrane Lipid Rafts. *Mol. Pharmacol.* **80**, 210–218 (2011).
52. Casiraghi, M. *et al.* Functional Modulation of a G Protein-Coupled Receptor Conformational Landscape in a Lipid Bilayer. *J. Am. Chem. Soc.* **138**, 11170–11175 (2016).
53. Manna, M. *et al.* Mechanism of allosteric regulation of β2-adrenergic receptor by cholesterol. *eLife* **5**, e18432 (2016).
54. Hanson, M. A. *et al.* A Specific Cholesterol Binding Site Is Established by the 2.8 Å Structure of the Human β2-Adrenergic Receptor. *Structure* **16**, 897–905 (2008).
55. Liu, W. *et al.* Structural Basis for Allosteric Regulation of GPCRs by Sodium Ions. *Science* **337**, 232–236 (2012).
56. Wacker, D. *et al.* Structural Features for Functional Selectivity at Serotonin Receptors. *Science* **340**, 615–619 (2013).
57. Manglik, A. *et al.* Crystal structure of the μ-opioid receptor bound to a morphinan antagonist. *Nature* **485**, 321–326 (2012).
58. Zhang, K. *et al.* Structure of the human P2Y12 receptor in complex with an antithrombotic drug. *Nature* **509**, 115–118 (2014).
59. Wu, H. *et al.* Structure of a class C GPCR metabotropic glutamate receptor 1 bound to an allosteric modulator. *Science* **344**, 58–64 (2014).
60. Burg, J. S. *et al.* Structural biology. Structural basis for chemokine recognition and activation of a viral G protein-coupled receptor. *Science* **347**, 1113–1117 (2015).

61. Taghon, G. J., Rowe, J. B., Kapolka, N. J. & Isom, D. G. Predictable cholesterol binding sites in GPCRs lack consensus motifs. *Structure* **29**, 499-506.e3 (2021).
62. Huang, S. K. *et al.* Allosteric modulation of the adenosine A2A receptor by cholesterol. *eLife* **11**, e73901 (2022).
63. Li, L. B., Vorobyov, I. & Allen, T. W. The role of membrane thickness in charged protein–lipid interactions. *Biochim. Biophys. Acta (BBA) - Biomembranes* **1818**, 135–145 (2012).
64. Mondal, S. *et al.* Membrane Driven Spatial Organization of GPCRs. *Sci. Rep.* **3**, 2909 (2013).
65. Róg, T. & Vattulainen, I. Cholesterol, sphingolipids, and glycolipids: What do we know about their role in raft-like membranes? *Chem. Phys. Lipids* **184**, 82–104 (2014).
66. Kulig, W. *et al.* How well does cholesteryl hemisuccinate mimic cholesterol in saturated phospholipid bilayers? *J. Mol. Model.* **20**, 2121 (2014).
67. Warne, T. *et al.* The structural basis for agonist and partial agonist action on a β1-adrenergic receptor. *Nature* **469**, 241–244 (2011).
68. Cang, X. *et al.* Cholesterol-β1AR interaction versus cholesterol-β2AR interaction. *Proteins: Structure, Function, and Bioinformatics* **82**, 760–770 (2014).
69. Quillin, M. L., Breyer, W. A., Griswold, I. J. & Matthews, B. W. Size versus polarizability in protein-ligand interactions: binding of noble gases within engineered cavities in phage T4 lysozyme11Edited by B. Honig. *J. Mol. Biol.* **302**, 955–977 (2000).
70. Guixà-González, R. *et al.* Membrane cholesterol access into a G-protein-coupled receptor. *Nat. Commun.* **8**, 14505 (2017).
71. Warne, T., Edwards, P. C., Doré, A. S., Leslie, A. G. W. & Tate, C. G. Molecular basis for high-affinity agonist binding in GPCRs. *Science* **364**, 775 (2019).
72. Liu, X. *et al.* An allosteric modulator binds to a conformational hub in the β2 adrenergic receptor. *Nat. Chem. Biol.* **16**, 749–755 (2020).
73. Lu, J. *et al.* Structural basis for the cooperative allosteric activation of the free fatty acid receptor GPR40. *Nat. Struct. Mol. Biol.* **24**, 570–577 (2017).
74. Zhang, D. *et al.* Two disparate ligand-binding sites in the human P2Y1 receptor. *Nature* **520**, 317–321 (2015).
75. Vial, C., Fung, C. Y. E., Goodall, A. H., Mahaut-Smith, M. P. & Evans, R. J. Differential sensitivity of human platelet P2X1 and P2Y1 receptors to disruption of lipid rafts. *Biochem. Biophys. Res. Commun.* **343**, 415–419 (2006).
76. Prangé, T. *et al.* Exploring hydrophobic sites in proteins with xenon or krypton. *Proteins: Structure, Function, and Bioinformatics* **30**, 61–73 (1998).
77. Paila, Y. D., Jindal, E., Goswami, S. K. & Chattopadhyay, A. Cholesterol depletion enhances adrenergic signaling in cardiac myocytes. *Biochim. Biophys. Acta (BBA) - Biomembranes* **1808**, 461–465 (2011).
78. Yeliseev, A. *et al.* Cholesterol as a modulator of cannabinoid receptor CB2 signaling. *Sci. Rep.* **11**, 3706 (2021).

79. Xiao, P. *et al.* Ligand recognition and allosteric regulation of DRD1-Gs signaling complexes. *Cell* **184**, 943-956.e18 (2021).
80. Robertson, N. *et al.* Structure of the complement C5a receptor bound to the extra-helical antagonist NDT9513727. *Nature* **553**, 111–114 (2018).
81. Cheng, R. K. Y. *et al.* Structural insight into allosteric modulation of protease-activated receptor 2. *Nature* **545**, 112–115 (2017).
82. Thal, D. M., Glukhova, A., Sexton, P. M. & Christopoulos, A. Structural insights into G-protein-coupled receptor allostery. *Nature* **559**, 45–53 (2018).
83. Keller, S. *et al.* High-Precision Isothermal Titration Calorimetry with Automated Peak-Shape Analysis. *Anal. Chem.* **84**, 5066–5073 (2012).
84. Rasmussen, S. G. F. *et al.* Structure of a nanobody-stabilized active state of the β2 adrenoceptor. *Nature* **469**, 175–180 (2011).
85. Warne, T., Serrano-Vega, M. J., Tate, C. G. & Schertler, G. F. X. Development and crystallization of a minimal thermostabilised G protein-coupled receptor. *Protein Expr. Purif.* **65**, 204–213 (2009).
86. McCoy, A. J. *et al.* Phaser crystallographic software. *J. Appl. Cryst.* **40**, 658–674 (2007).
87. Winn, M. D. *et al.* Overview of the CCP4 suite and current developments. *Acta Cryst. D* **67**, 235–242 (2011).
88. Vonrhein, C. *et al.* Data processing and analysis with the autoPROC toolbox. *Acta Cryst. D* **67**, 293–302 (2011).
89. Kabsch, W. XDS. *Acta Crystallogr. D Biol. Crystallogr.* **66**, 125–132 (2010).
90. Sheldrick, G. M. Experimental phasing with SHELXC/D/E: combining chain tracing with density modification. *Acta Cryst. D* **66**, 479–485 (2010).
91. Thorn, A. & Sheldrick, G. M. ANODE: anomalous and heavy-atom density calculation. *J. Appl. Crystallogr.* **44**, 1285–1287 (2011).
92. Liebschner, D. *et al.* Macromolecular structure determination using X-rays, neutrons and electrons: recent developments in Phenix. *Acta Cryst D* **75**, 861–877 (2019).
93. Schrödinger, LLC. The PyMOL Molecular Graphics System, Version 1.8. (2015).
94. Ho, B. K. & Gruswitz, F. HOLLOW: Generating Accurate Representations of Channel and Interior Surfaces in Molecular Structures. *BMC Struct. Biol.* **8**, 49 (2008).
95. Sklenář, V. & Bax, A. Spin-echo water suppression for the generation of pure-phase two-dimensional NMR spectra. *J. Magn. Reson.* **74**, 469–479 (1987).
96. Scheuermann, T. H. & Brautigam, C. A. High-precision, automated integration of multiple isothermal titration calorimetric thermograms: new features of NITPIC. *Methods* **76**, 87–98 (2015).
97. Zhao, H., Piszczek, G. & Schuck, P. SEDPHAT--a platform for global ITC analysis and global multi-method analysis of molecular interactions. *Methods* **76**, 137–148 (2015).
98. Brautigam, C. A. Calculations and Publication-Quality Illustrations for Analytical Ultracentrifugation Data. *Methods Enzymol.* **562**, 109–133 (2015).